eXPRESS Polymer Letters Vol.5, No.5 (2011) 428–448
Available online at www.expresspolymlett.com
DOI: 10.3144/expresspolymlett.2011.42

Effect of surfactant alkyl chain length on the dispersion, and thermal and dynamic mechanical properties of LDPE/organo-LDH composites

N. Muksing[1], *R. Magaraphan*[1], *S. Coiai*[2*], *E. Passaglia*[2]

[1]Polymer Processing and Polymer Nanomaterials Research Unit, Center for Petroleum, Petrochemicals and Advanced Materials, The Petroleum and Petrochemical College, Chulalongkorn University, Bangkok 10330, Thailand
[2]CNR-ICCOM UOS Pisa, c/o Department of Chemistry and Industrial Chemistry, University of Pisa, Via Risorgimento 35, 56126 Pisa, Italy

Received 10 September 2010; accepted in revised form 4 December 2010

Abstract. Low density polyethylene/layered double hydroxide (LDH) composites were prepared via melt compounding using different kinds of organo-LDHs and polyethylene-grafted maleic anhydride as the compatibilizer. The organo-LDHs were successfully prepared by converting a commercial MgAl-carbonate LDH into a MgAl-nitrate LDH, which was later modified by anion exchange with linear and branched sodium alkyl sulfates having different alkyl chain lengths (n_c = 6, 12 and 20). It was observed that, depending on the size of the surfactant alkyl chain, different degrees of polymer chain intercalation were achieved, which is a function of the interlayer distance of the organo-LDHs, of the packing level of the alkyl chains, and of the different interaction levels between the surfactant and the polymer chains. In particular, when the number of carbon atoms of the surfactant alkyl chain is larger than 12, the intercalation of polymer chains in the interlayer space and depression of the formation of large aggregates of organo-LDH platelets are favored. A remarkable improvement of the thermal-oxidative degradation was evidenced for all of the composites; whereas only a slight increase of the crystallization temperature and no significant changes of both melting temperature and degree of crystallinity were achieved. By thermodynamic mechanical analysis, it was evidenced that a softening of the matrix is may be due to the plasticizing effect of the surfactant.

Keywords: *polymer composites, organo-LDHs, morphological features, thermal properties*

1. Introduction

Layered double hydroxides (LDHs), commonly known as hydrotalcite-like compounds or anionic clays, are a class of host−guest materials whose general formula is $[M^{2+}_{1-x}M^{3+}_{x}(OH)_2]^{x+}A^{n-}_{x/n}\cdot mH_2O$, where M^{2+} is a divalent metal ion (i.e. Mg^{2+}, Zn^{2+}, etc.), M^{3+} is a trivalent metal ion (i.e. Al^{3+}, Cr^{3+}, etc.), A is an anion with valency n (i.e. CO_3^{2-}, Cl^-, NO_3^-, etc.) or an organic anion, m is the number of moles of water per formula weight of compound, and x is a stoichiometric coefficient, generally ranging between 0.2 and 0.4, which determines the layer charge density and the anion exchange capacity [1–3].

LDHs are structurally similar to the mineral brucite $[Mg(OH)_2]$ with a fraction of the M^{2+} ions being replaced by M^{3+} ions. Such replacement results in a net positive charge on the octahedral layers, which is balanced by the anions located in the interlayer region where the hydration water molecules are also present [3, 4].

*Corresponding author, e-mail: serena.coiai@ns.dcci.unipi.it
© BME-PT

Owing to their highly tunable and unique anion exchange properties, LDHs are being considered as new emerging layered host materials that can be tailored to accommodate a wide range of guest molecules to create novel solids with desirable physical and chemical properties controlled by host−guest and guest−guest interactions [5]. As layered hosts, LDHs have been used in many potential applications, such as catalysts, ceramic precursors, ion exchangers, absorbents, medicine stabilizers, and for controlled release of anions [6–13]. Very recently, their potential as nanofillers for preparing polymer nanocomposites has received considerable attention from both academic and industrial points of view. In contrast to more conventional layered silicates (i.e. MMT), LDHs possess certain inherent advantages; for example, being mostly of synthetic origin, their composition and properties can be modulated by simply changing the type and the molar ratio of the metal ion pairs during the preparation. In addition, the unique positive charge of LDH crystal layers provides a greater flexibility in selecting the most suitable organic modifiers. However, the hydrophilic nature, the strong interlayer electrostatic interactions, and the small intergallery space (around 0.28 nm) make them incompatible with hydrophobic polymers. For this reason, it is necessary to modify the LDH surface, usually with organic anions [14], in order to minimize the attractive forces between the layers, and to increase the interlayer distance and hydrophobicity of LDH, aiming to obtain a good dispersion in polymer matrices.

There are several methods reported in the literature for preparing organo-modified LDHs, i.e. anion-exchange of a precursor LDH, regeneration, thermal reaction, direct synthesis by coprecipitation, and the more recent one-step synthesis method [15–17]. Among all of the methods described, anion exchange is one of the more commonly used and several anionic species, such as phosphates, carboxylates, sulfonates, and sulfates, have been used [18]. Actually, the exchange reaction is controlled by the selectivity of the layered host for the different anions, and in a previous work by Miyata *et al.* [19], it was demonstrated that the selectivity scale of exchangeable anions is as follows:

$CO_3^{2-} > SO_4^{2-} >> OH^- > F^- > Cl^- > Br^- > NO_3^- > ClO_4^-$.

LDHs containing ClO_4^-, NO_3^-, or even Cl^- are generally used as precursors for up taking long-chain organic anions owing to their large anion-exchanging capacity.

LDH−based polymer nanocomposites have been extensively investigated with a large number of polymers, including, epoxy resins [20], polyamide [21], poly(ethylene terepthalate) [22], poly(vinyl alcohol) [23], poly(lactic acid) [24], poly(ε-caprolactone) [25], polypropylene [26–30], and polyethylene [15, 31–40]. Much attention has been focused on preparing LDH polyethylene (PE)-based nanocomposites due to the good balance between processability, mechanical properties, and chemical resistance of this thermoplastic polymer, very suitable for packaging and engineering applications. In particular, LDH PE−based nanocomposites were prepared by solution intercalation [31–34] and melting processes [35–40]. Costa and coworkers [35, 39] first reported the preparation of intercalated/flocculated LDPE/(dodecyl benzene sulphonate, DBS)-LDH nanocomposites using a melt intercalation process. A complex morphological feature of dispersed LDH particles was observed, with the particles mostly located in the form of thin platelets and agglomerates. Rheological studies of these nanocomposites evidenced a significant change of the linear viscoelastic response in the low frequency region with respect to the matrix due to the formation of a network-like structure via the interaction between the LDH particles and the polymer chains, even if the morphological analysis by X-ray diffraction (XRD) and transmission electron microscopy (TEM) did not give evidence of homogeneous dispersion and perfect exfoliation of DBS-LDH particles. Nonetheless, both thermal stability and fire resistance properties were significantly enhanced [36], most likely due to the barrier effect of LDH layers on the oxygen diffusion, thus preserving PE chain segments from thermal oxidation. Similar results were also achieved in the case of LLDPE/dodecyl sulphate (DS)-LDH nanocomposites [37] and PE/ stearate-LDH nanocomposites [38].

Even though it has been demonstrated that the organic modification of LDH is sufficient to achieve the intercalation of PE chains between the layers [41], the use of a compatibilizer, such as a polyethylene functionalized with maleic anhydride groups (PEMAH), is necessary to improve the interactions between the polymer and the LDH and to favor the formation of composites with a stable morphology.

Costa *et al.* [39] prepared PE/LDH composites using an unmodified PE and a PE functionalized with MAH, both as the matrix; in particular, it was investigated how the chemical compatibility of the polymer matrix with LDH influences the morphology of the composites and the rheological properties. The scanning electron microscopy (SEM) analysis evidenced that platelets were well coated by the functionalized polymer, while the formation of structural associations, or clusters, was associated with the presence of the unmodified PE. A different behavior of rheological parameters vs. temperature, due to a deviation from the liquid-like low frequency toward a pseudo solid-like flow, was also observed in the presence of the functionalized PE, originating from the differences between the polymer-particle and particle-particle chemical interactions [42].

In the framework of a study of the role of interfacial effects/interactions in the preparation of nanocomposites, we report results about the morphology and properties of LDPE/organo-LDH composites prepared by changing the type of anion used for modifying the LDH. LDH-CO_3 was first converted to LDH-NO_3 for facilitating the organo-modification by anion exchange. Then, three different organo-LDHs were prepared with linear and branched alkyl sulfates having different alkyl chain lengths (n_c = 6, 12 and 20, which is the number of carbon atoms of the main alkyl chain), and the products were characterized by XRD, Fourier transform infrared spectroscopy (FTIR), SEM, and thermogravimetry (TGA). Finally, LDPE composites were prepared by melt processing with all of the organo-LDHs and using a PEMAH as compatibilizer of the system. The morphology, and thermal and thermo-mechanical properties of such materials were investigated in order to evaluate the effect of the dispersion of LDH platelets in the polymer matrix on the final properties.

2. Experimental part

2.1. Materials

Low-density polyethylene (LDPE, Riblene FL34), with a density of 0.924 g/cm^3 and a melt flow index of 2.1 g/10 min (190°C, 2.16 kg) was purchased from Polimeri Europa S.p.A (Mantova, Italy). Polyethylene, functionalized with maleic anhydride (PEMAH) UL EP Compoline® by Auserpolimeri S.r.l. (Lucca, Italy), having a melt flow index of 2.5 g/10 min (190°C, 2.16 kg) and an amount of maleic anhydride grafted groups of 0.5 to 1.0 wt%, was used as the compatibilizer. MgAl hydroxy carbonate, PURAL MG63HT (LDH-CO_3), having the following molecular formula,
$Mg_{0.66}Al_{0.34}(OH)_2(CO_3)_{0.17}\cdot 0.62H_2O$ as previously determined [28], was kindly supplied by Sasol GmbH (Hamburg, Germany). 2-ethylhexyl sulphate, dodecyl sulphate, and eicosyl sulfate were purchased from Aldrich Chemical Company (Steinheim, Germany). The chemical structures are shown in Figure 1.

2.2. Synthesis of Mg/Al LDH-NO_3 and organo-LDHs

The Mg/Al layered double hydroxide, labeled as LDH-CO_3, was used as the precursor. The nitrate form, with the formula
$[Mg_{0.66}Al_{0.34}(OH)_2](NO_3)_{0.34}\cdot 0.44H_2O]$, labeled as LDH-$NO_3$, was obtained by titration at room temperature of the LDH-CO_3 dispersed in a 1M $NaNO_3$ aqueous solution (mass/volume = 2 g/100 ml) with

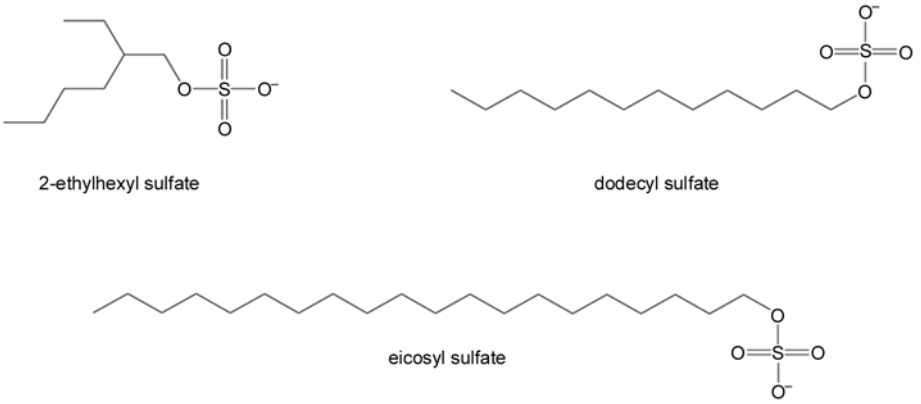

Figure 1. Chemical structure of anionic surfactant guest molecules used for preparing the organo-LDHs

a 1M HNO_3. After titration, the white solid was washed several times with CO_2-free deionized water and dried overnight at 60°C in a vacuum oven [43]. The calculated anion-exchange capacity (AEC) of the LDH-NO_3 was 3.81 mmol of NO_3^-/g, calculated as follows: AEC = $x/M_w \cdot 10^3$ (mequiv/g), where M_w and x are the molecular weight and the layer charge per octahedral unit, respectively [44, 45].

The organo-LDHs were synthesized via anion-exchange reaction. Firstly, for each organo-LDH, an amount of surfactant corresponding to 1.5 times the AEC of the LDH-NO_3 was dissolved in 100 ml of CO_2-free deionized water and heated at 70°C until a clear solution was obtained. The pH of the solution was maintained at 10 by using 1M NaOH solution. Secondly, 1 g of the LDH-NO_3 was added to the surfactant solution, followed by ultrasound treatment for 15 min. The mixture was magnetically stirred for 24 h at 70°C in nitrogen atmosphere. Then the resulting organo-LDHs were first separated by centrifugation at 6000×g for 10 min, washed several times with CO_2-free deionized water until pH = 7, and finally dried at 60°C under N_2 atmosphere till constant weight. The organo-LDHs were labeled as LDH-C6, LDH-C12, and LDH-C20 having 2-ethylhexyl sulfate, dodecyl sulfate, and eicosyl sulfate, respectively, as interlayer anions.

2.3. Preparation of LDPE/organo-LDH composites

LDPE composites with different organo-LDHs were prepared in an internal batch mixer (Plastograph PL2100, Brabender, Duisburg, Germany) 30 ml chamber at 180°C using a screw speed of 80 rpm. In the first step, LDPE and PEMAH were melt blended in the mixing chamber for 4 min until achieving a constant torque value, then the desired amount and type of organo-LDH was added and compounded for 16 min. The amount of clay was fixed at 2.5 wt% with respect to the polymer matrix in the case of LDH-C6 and LDH-C12, and 1.5 wt% for LDH-20, whereas the PEMAH compatibilizer was added in the same amount as the organo-LDH. In the case of the LDH-C12, a second composite was prepared by adding 5 wt% LDH-C12 with respect to the total amount of polymers to obtain LDPE/LDH-C12_5%. The exact formulation for each composite is given in Table 2.

Table 1. Reflections of the *<00l>* series, interlayer spacing values, and chemical formulae of the LDH-CO_3, LDH-NO_3, and organo-LDHs modified with various types of alkyl sulfate surfactants

Sample	No. of carbon alkyl chain length (n_c)	Reflections of the *<00l>* series [°] /d-spacing [nm]			Arrangement in the interlayer LDH	B^a (FWHM, rad.)	Chemical formulae[b]
		<003>	<006>	<009>			
LDH-CO_3	–	9.9 (0.89)	23.4 (0.38)	34.6 (0.26)	–	0.24	$Mg_{0.66}Al_{0.34}(OH)_2(CO_3)_{0.17}{\cdot}0.62H_2O$
LDH-NO_3	–	9.9 (0.89)	19.9 (0.45)	34.6 (0.26)	–	0.25	$Mg_{0.66}Al_{0.34}(OH)_2(NO_3)_{0.34}{\cdot}0.44H_2O$
LDH-C6	6	4.2 (2.12)	8.5 (1.04)	12.6 (0.74)	monolayer	0.52	$Mg_{0.66}Al_{0.34}(OH)_2(CO_3)_{0.092}(C_8H_{17}SO_4)_{0.157}{\cdot}0.48H_2O$
LDH-C12	12	3.6 (2.42)	7.3 (1.22)	10.9 (0.81)	monolayer	0.38	$Mg_{0.66}Al_{0.34}(OH)_2(CO_3)_{0.101}(C_{12}H_{25}SO_4)_{0.139}{\cdot}0.52H_2O$
LDH-C20	20	2.7 (3.25)	5.5 (1.61)	8.3 (1.07)	monolayer	0.42	$Mg_{0.66}Al_{0.34}(OH)_2(CO_3)_{0.062}(C_{20}H_{41}SO_4)_{0.216}{\cdot}0.65H_2O$

[a]*B* is the full-width at half-maxima (FWHM, rad.) obtained from XRD results.

[b]The chemical formulae of the LDH-CO_3, LDH-NO_3, and organo-LDHs were determined by combining the results of ICP-OES, elemental analysis, and TGA analysis.

Table 2. Composition of LDPE/organo-LDH composites and their thermal properties

Composites (LDPE/PEMAH/Organo-LDH composition)	$T_{10\%}$ [°C]	$T_{50\%}$ [°C]	T_{max} [°C]	ΔT_{max} [°C]	T_c, peak [°C]	T_m, peak [°C]	ΔH_m [J/g]	χ_c[a]	Residue[b] [%]
LDPE (100)	376.0	414.6	434.2	–	85.6	108.8	132.2	45.1	0.31
LDPE/PEMAH (97.5/2.5)	380.0	417.6	431.5	–	84.9	112.3	130.5	44.5	0.48
LDPE/LDH-C6 (97.5/2.5/2.5)	371.8	443.0	464.2	32.7	86.4	110.3	126.1	44.1	1.35
LDPE/LDH-C12 (97.5/2.5/2.5)	370.7	433.3	452.1	20.6	84.4	112.2	125.6	44.0	1.09
LDPE/LDH-C20 (98.5/1.5/1.5)	384.9	440.4	456.8	25.3	86.9	109.6	130.7	45.3	0.68
LDPE/LDH-C12_5% (95/5/5)	367.8	434.7	457.0	25.5	84.5	110.0	119.7	43.0	2.13

[a]Calculated as follows: $\chi_c=\Delta H_m/(1-x)\Delta H_m^0\cdot 100$, where ΔH_m is the experimental melting enthalpy, $(1-x)$ is the polyethylene fraction by weight in the composite, and ΔH_m^0 is the melting enthalpy of infinite polyethylene crystal (293 J/g).
[b]Residue at 900°C obtained from TGA analysis.

2.4. Characterizations

X-ray diffraction (XRD) patterns of LDH-CO_3, LDH-NO_3, organo-LDHs, and their LDPE composites were recorded by using a Kristalloflex 810, (Siemens, Karlsruhe, Germany) diffractometer (CuK_α radiation, λ = 0.15406 nm) in the 2θ region of 1.5 to 40° at the scanning rate of 0.016°/min. The crystallite size of LDHs was calculated using the Scherrer Equation (1):

$$L = \frac{\lambda \cdot \kappa}{B \cdot \cos\theta} \quad (1)$$

where L [nm] is the thickness of the crystallite in the direction perpendicular to the plane metal hydroxide sheet in LDH materials, κ is a factor between 0.87 and 1.00, B is the full-width at half-maxima (FWHM, rad) and θ is the scattering angle [°].

Fourier transform infrared (FT-IR) spectra of the LDH-CO_3, LDH-NO_3, and organo-LDHs were recorded over the wavenumber range 450 to 4000 cm^{-1} using a spectrophotometer (Model 1760-X, PerkinElmer, Waltham, Massachusetts, USA). The spectra were obtained by mixing the sample with potassium bromide powder.

The thermogravimetric analysis (TGA) of the LDH-CO_3, LDH-NO_3, organo-LDHs, and LDPE composites was performed (Model TGA/SDTA 851^e, Mettler-Toledo GmbH, Schwerzenbach, Switzerland). Samples (~10 mg) were placed in alumina sample pans and runs were carried out at the standard rate of 10°C/min from 25 to 900°C under air flow (60 ml/min).

The Mg/Al ratios of the LDH-NO_3 and organo-LDHs were determined by inductively coupled plasma atomic emission spectrometry (ICP-OES) (Varian Vista MPX, Varian, Palo Alto, California, USA) using a Varian Vista MPX spectrometer, as previously reported [28]. For this analysis samples were dissolved in a nitric acid solution. In this way it was determined the stoichiometric coefficient x of the LDH general formula $[M^{2+}_{1-x}Al^{3+}_x(OH)_2]^{x+}A^{n-}_{x/n}\cdot mH_2O$. Carbon, hydrogen, and sulfur elemental analyses of the organo-LDHs were determined by a CHNS elementary analyzer (TruSpec®, LECO Corporation, St Joseph, Michigan, USA). The analyses yielded the following results:

LDH-C6: 55.98% C, 7.52% H, 5.46% S;
LDH-C12: 54.72% C, 7.11% H, 5.15% S;
LDH-C20: 56.59% C, 7.51% H, 5.80% S.

Accordingly, the intercalation amount of alkyl sulfate surfactants into the LDH interlayers was calculated. Finally, the moles of water per formula weight of compound, m, were estimated by the first step of degradation of the TGA. The chemical formulae of the organo-LDHs, calculated by combining all these information are given in Table 1.

The morphological features of the LDH-CO_3, LDH-NO_3, and organo-LDHs were studied using a scanning electron microscope (FE-SEM) (S-4800, Hitachi High-Technologies Corporation, Ibaraki-ken, Japan). The powdered samples were first spread on a sample button using conducting cement, while the composite samples were dipped and fractured in liquid nitrogen before putting them on the sample button. Then, all of the samples were sputtered with platinum before viewing under the electron microscope operating at 3 kV.

The transmission electron microscopy (TEM) (Zeiss EM 900 microscope, Carl Zeiss, Oberkochen, Germany) was performed operating at an acceleration voltage of 80 kV. Ultrathin sections (about 50 nm thick) of compression-moulded plaques were prepared by a cryoultramicrotome (Leica EM FSC,

Leica Mikrosystems GmbH, Vienna, Austria) equipped with a diamond knife, keeping the samples at –145°C.

Differential scanning calorimetry (DSC) measurements were carried out on 5–10 mg samples by using a calorimeter equipped with a CCA7 liquid nitrogen cooling device (DSC7, PerkinElmer, Waltham, Massachusetts, USA). The melting/crystallization behaviour of LDPE, LDPE/PEMAH blends and organo-LDH composites was investigated in the temperature range from –30 to 200°C at the scanning rate of 20°C/min under nitrogen flow. Indium (T_m = 156.95°C; ΔH_m = 28.49 J/°C) and zinc (T_m = 419.50°C) were used as calibration standards. The crystallinity degree from DSC was calculated according to the Equation (2):

$$x_c = \frac{\Delta H_m}{(1-x)\cdot \Delta H_m^0}\cdot 100 \qquad (2)$$

where ΔH_m is the experimental melting enthalpy, $(1-x)$ is the polyethylene fraction by weight in the composite and ΔH_m^0 is the melting enthalpy of an infinite polyethylene crystal (293 J/g).

The thermo-mechanical properties of materials were investigated by dynamic mechanical thermal analysis (DMTA) (DMA7e, PerkinElmer, Waltham, Massachusetts, USA) in three-point bending geometry. Thermograms were obtained at a heating rate of 5°C/min and 1 Hz frequency in the temperature range of –150 to 50°C.

Specimens of the composites for XRD, TEM and DMTA (2×1×0.2 cm) analyses were prepared at 190°C by using a laboratory hot-press (Carver 3851-0, Carver®, Wabash, Indiana, USA).

3. Results and discussion

3.1. Preparation and characterization of the organo-LDH particles

To facilitate the exchange process with organic surfactants, the LDH carbonate form (LDH-CO_3) was converted into nitrate (LDH-NO_3) following the method described by Miyata [19]. The XRD pattern of the LDH-NO_3 evidences the shift of all diffraction maxima to lower angles and, in particular, the (003) basal reflection from 2θ = 11.7° to 2θ = 9.9°, corresponding to an enlargement of the basal spacing (d_{003}) from 0.76 to 0.89 nm (Figure 2a). Moreover, the FTIR spectrum of the LDH-NO_3 (Figure 2b) shows peaks at 1384 and 839 cm^{-1}, due to the v_3 and v_2 vibration modes, respectively, of the NO_3^- [43], in addition to adsorption peaks at 670 and 550 cm^{-1} (Al–OH and Mg–OH translation modes), and a broad adsorption peak at 3459 cm^{-1}, associated with the –OH stretching [46].

The XRD patterns of the organo-LDHs modified with anionic surfactants having alkyl chains of different lengths, two linear and one branched, are shown in Figure 3a. For all of the samples, it was clear that there was a further shift toward lower angles of the (003) basal reflection with the increasing number of carbon atoms of the surfactant alkyl chain (n_c), which is consistent with an enlargement of the interlayer distance from 0.89 to 2.12, 2.42 and 3.25 nm for n_c = 6, 12 and 20, respectively (Table 1). Moreover, higher order reflection peaks (00l), due to the formation of well-ordered guest intercalated LDH layers, are shown in the XRD patterns. Nonetheless, even if the anion exchange was carried out under nitrogen atmosphere to prevent

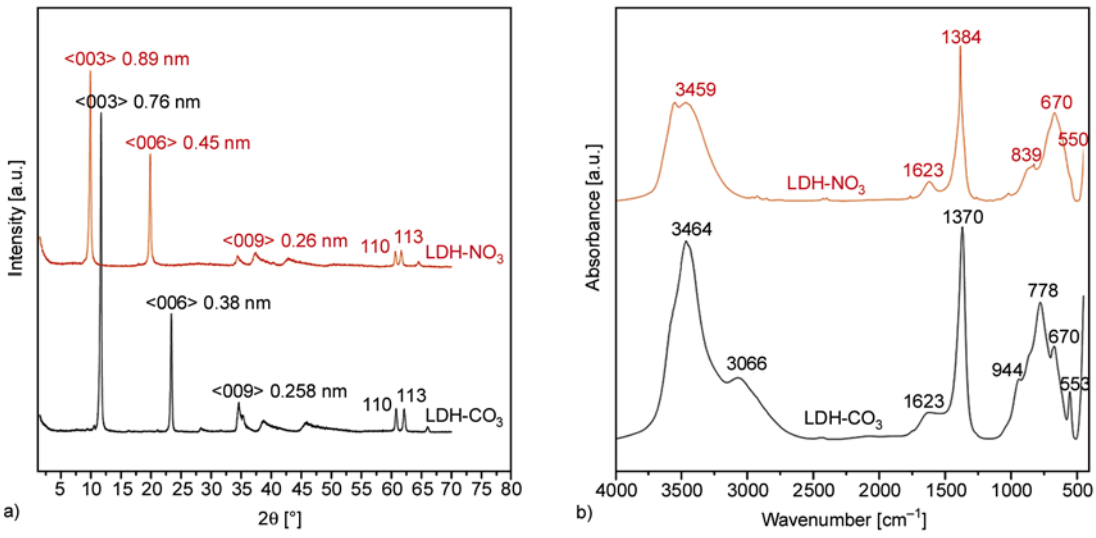

Figure 2. XRD patterns (a) and FTIR spectra (b) of LDH-NO_3 and LDH-CO_3

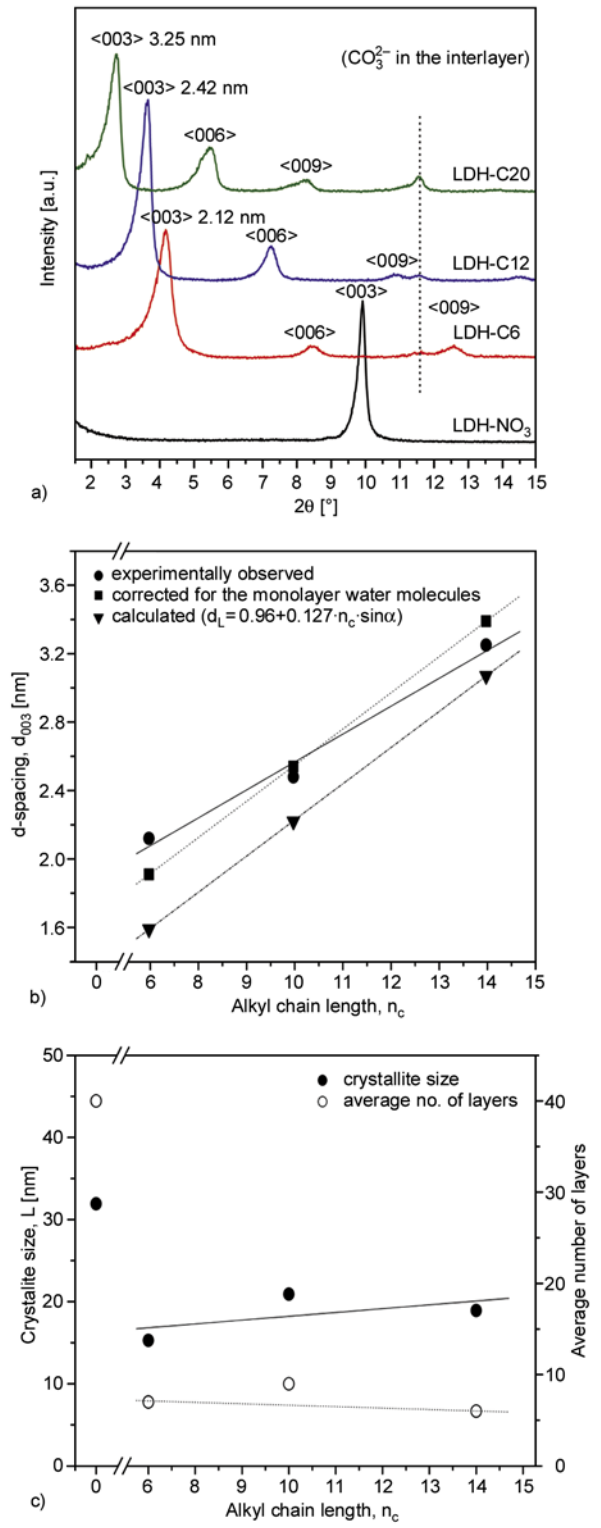

Figure 3. Effect of alkyl chain length (n_c) of sulfate surfactants on: (a) XRD patterns of organo-LDHs, (b) *d*-spacing and alkyl chain arrangement between the LDH layers, and (c) average crystallite size

carbonate contamination, a weak peak at $2\theta \cong 11.5°$ (0.77 nm), related to the co-intercalation of carbonate anions, still exists for all of the samples. A perpendicular orientation of surfactants in organo-LDHs has been observed in previous studies [47–49]. Indeed, due to the small equivalent area of LDHs, the surfactants form generally mono- or bimolecular films instead of lying flat on the interlamellar surfaces. Based on these investigations, which were carried out for a wide range of LDHs and surfactants, the relation for predicting the interlayer distance in the case of primary alkyl sulfates with monolayer or bilayer arrangement of the surfactant in the interlayer space is given by Equations (3) and (4), respectively [48–51]:

$$\text{monolayers:} \quad d_L\,[\text{nm}] = 0.96 + 0.127 \cdot n_c \cdot \sin\alpha \qquad (3)$$

$$\text{bilayers:} \quad d_L\,[\text{nm}] = 1.42 + 0.254 \cdot n_c \cdot \sin\alpha \qquad (4)$$

where d_L is the basal spacing in nm, n_c is the number of carbon atoms in the alkyl chain of the surfactant, and α is the tilt angle of the alkyl chain from the normal of the metal hydroxide sheet. In particular, it has been demonstrated that in the case of alkyl sulfate anions the value of the α angle is 56° [47–49, 52, 53]; moreover, a layer of adsorbed water molecules is generally present in between the hydrocarbon chain end of the surfactant and the metal hydroxide layer [47, 48, 51, 52] which takes up about 0.3–0.5 nm. In particular, a value of 0.32 nm for the adsorbed layer of water molecules was reported in the case of LDH modified with dodecyl benzene sulfonate anions. According to these results, the experimental interlayer distances of organo-LDHs were compared with predicting values estimated by considering a monolayer arrangement of the alkyl sulfate ions between the layers of LDHs (Figure 3b). The calculated d_L values were corrected by considering an adsorbed layer of water molecules of 0.32 nm. The linear relationship existing between the d_L values and the number of carbon atoms of the surfactant alkyl chains (Figure 3b) is consistent with the hypothesis of a monolayer arrangement of all surfactants between the LDH layers. A close similarity between experimental and calculated values was obtained in the case of LDH-C12, whereas for both LDH-C6 and LDH-C20, small differences were observed which could be due to a different tilt angle of the surfactant alkyl chains and/or a different amount of the water adsorbed layer with respect to those considered for the valuation. In particular, for the case of LDH-C6 the ethyl

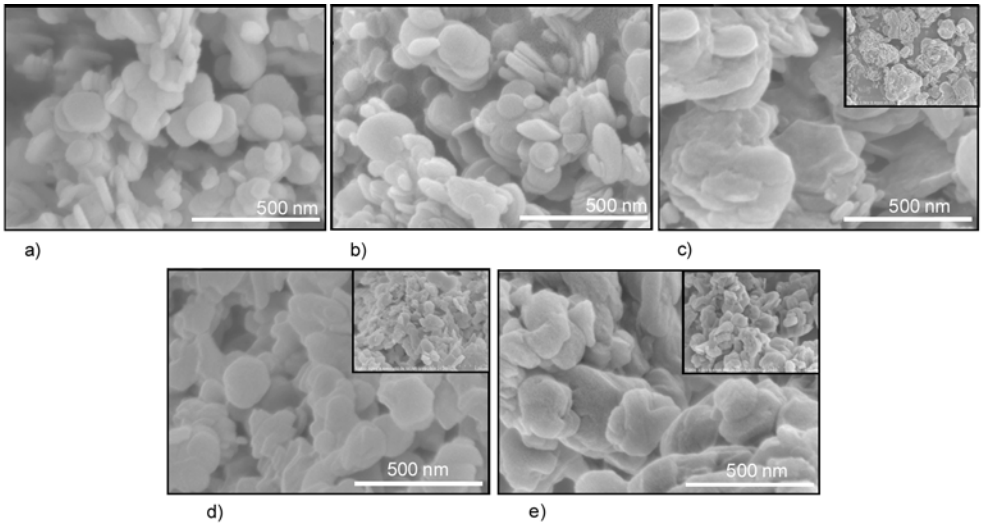

Figure 4. SEM micrographs of (a) LDH-CO_3, (b) LDH-NO_3, (c) LDH-C_6, (d) LDH-C12 and (e) LDH-C20 at low and high magnifications

branched chain of the surfactant could induce steric hindrance, thus changing the interlayer orientation to a higher tilt angle. By analyzing the XRD patterns (Figure 3c), it appears that both the average crystallite size and the average number of metal hydroxide layers of the organo-LDHs (calculated from the ratio of the average crystallite size and the *d*-spacing) decrease with respect to the LDH-NO_3, and there is no linear relation with n_c.

The morphological features of LDH-CO_3, LDH-NO_3, and organo-LDHs are presented in Figure 4a–e. The high magnification SEM micrograph of the LDH-CO_3 (Figure 4a) reveals a stacking of hexagonal plate-like particles with a highly anisometric nature, where the lateral dimension varies from 100 to 200 nm and the thickness is less than 100 nm. After the exchange of carbonate with nitrate anions, the particle morphology is substantially unchanged (Figure 4b), whereas the nitrate exchange with the organic surfactants leads to clear variation.

In particular, for the smallest surfactant alkyl chain (n_c = 6, Figure 4c), the stacking structure of the plate-like particles seems to be partially lost. Actually, the particles appear in aggregated form (see the inset picture) with a size of □500 nm and a rougher surface than the unmodified particles. The irregular particle morphology in our case may come from the ethyl-branched structure of the surfactant probably hindering the ordering of the LDH layers, as similarly observed [52]. Most likely, the stacks tend to connect to each other, probably via hydrophobic interactions [54]. When n_c is increased to 12 (Figure 4d), well-stacked hexagonal particles reappear, whereas for n_c equal to 20 (Figure 4e), the particle morphology is somewhat changed as compared to the others. Indeed, the LDH-C20 particles arrange themselves in a non-uniform stacking of irregular hexagonal plate-like particles. Also, there appears to be an uneven surface and unshaped edges, probably as a consequence of the excess of anionic surfactants draped over the outer particle surfaces [52, 54, 55].

The successful exchange of these surfactants into the LDH layers was also confirmed by the FTIR spectra (Figure 5). The organo-LDHs show absorption peaks at 1220 and 1065 cm^{-1}, corresponding to symmetric and asymmetric S=O vibration of the

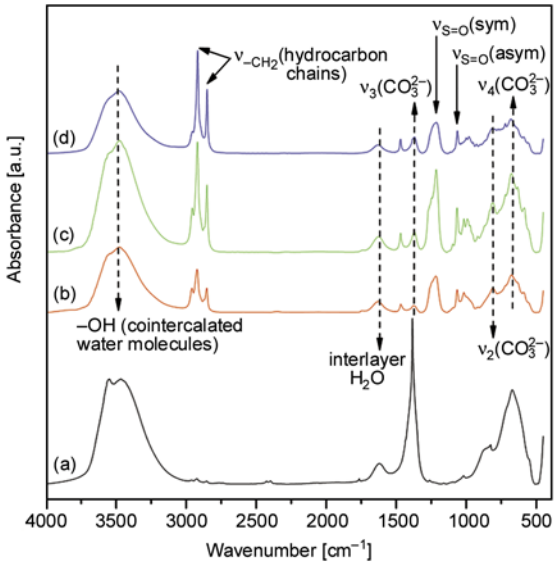

Figure 5. FTIR spectra of (a) LDH-NO_3, (b) LDH-C6, (c) LDH-C12 and (d) LDH-C20

sulfate group, as well as absorption peaks at 2850–2965 cm^{-1}, which are due to the $–CH_2$ stretching of the hydrocarbon chains [37, 56]. The appearance of broad characteristic peaks of CO_3^{2-} ions at 1370 (ν_3), 820 (ν_2), and 680 cm^{-1} (ν_4), suggests there are a few carbonate ions remaining between the layers, in agreement with XRD results [3, 37]. The presence of interlayer water molecules in the organo-LDHs was evidenced by the shoulder absorption band at 1632 cm^{-1}, due to the H_2O bending vibration.

The TGA/DTG curves of the LDH-NO_3 and the organo-LDHs are shown in Figure 6. It can be seen that the LDH-NO_3 exhibits a two step decomposition process. The first weight loss step, up to 300°C, is attributed to the loss of adsorbed and interlayer water molecules (~9%), whereas the second weight loss step, between 300 and 750°C (~37%), corresponds to the loss of the interlayer nitrate ions and to the dehydroxylation of the metal hydroxide layers [57]. The thermal decomposition behavior of all of the organo-LDHs mainly takes place in four steps. The first decomposition step, up to 180°C (~10%), corresponds to the loss of the surface water molecules and crystallization water located in the interlayer region. This step shifts to lower temperatures as compared to the unmodified LDH; this shift is due to the fact that the interaction between the interlayer water molecules and the hydroxide layers was greatly reduced by the incorporation of surfactant molecules [36]. In the temperature range of 180 to 800°C, there is a combination of three degradation steps (accounting for about 50% of the sample mass loss) which are due to the degradation of the samples up to the formation of metal oxides. This combinatorial degradation stage and the related exothermic effect involve more processes: the decomposition of intercalated alkyl sulfate surfactants (180 to 260°C) [36], the loss of some interlayer carbonate ions interfering with partial dehydroxylation of the layered LDH (260 to 500°C), and then the complete dehydroxylation process of the layered LDH. Among the organo-LDHs, LDH-C20 exhibits a maximum thermal stability, most likely due to the higher stability of the eicosyl sulfate compared to the other surfactants.

Moreover, as expected, the smallest amount of residue at 900°C was obtained for this sample which

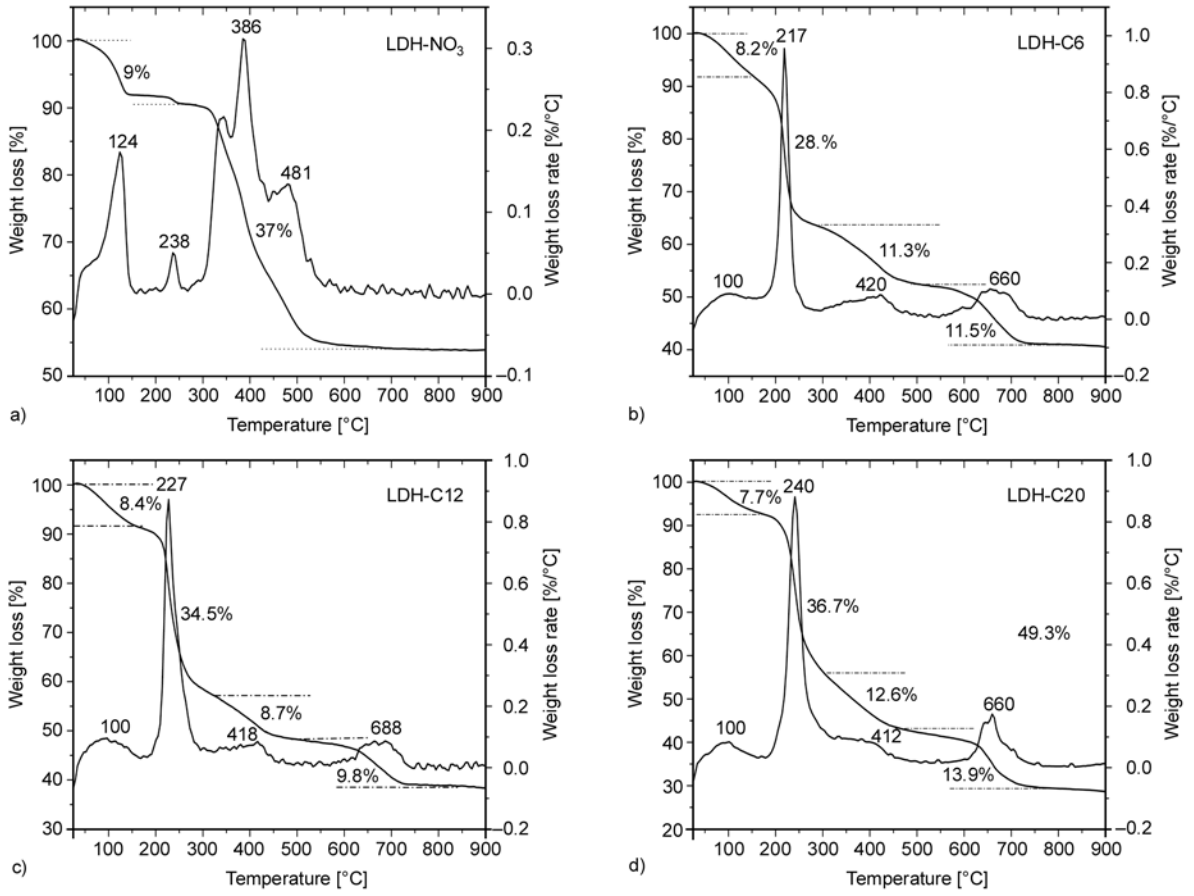

Figure 6. TGA/DTG curves of (a) LDH-NO_3, (b) LDH-C6, (c) LDH-C12 and (d) LDH-C20

contains the surfactant with the highest molecular weight.

3.2. Preparation and characterization of the LDPE/organo-LDH composites

After the addition of the organo-LDH to the molten matrix, no significant changes in the torque-versus-time plot were observed for any of the samples (Figure 7a). Generally, in the case of organo-clays, it is reported that fracturing of clay particles into smaller aggregates, and delamination lead to a gradual increase of the melt viscosity, thus determining a torque raise [58]. In our case, the unchanged torque behavior could be due to the plasticizing effect of the high surfactant amount present in the organo-LDHs, which could suppress any effect of reinforcement.

The XRD patterns of the composites in the range $2\theta = 1.5$ to 10° are shown in Figure 7b. In the case of the LDPE/LDH-C6 sample, a (003) basal reflection at $2\theta = 3.9°$ (2.3 nm), very close to the value of pure LDH-C6, was observed, thus suggesting that the LDH-C6 was probably not dispersed in the LDPE matrix. On the other hand, in the case of the LDPE/LDH-C12 and LDPE/LDH-C20 composites, (003) basal reflections of low intensity at $2\theta = 3.18°$ (2.8 nm) and $2\theta = 2.28°$ (3.9 nm), respectively, were observed. For these two samples, the polymer chains were intercalated, and it cannot be excluded that a partially exfoliated/intercalated mixed morphology, as well as small or disordered stacks of platelets, was formed. Moreover, it was observed that the higher order basal reflection (i.e. <006> and <009>) distinctly reduced or disappeared, further evidencing that the well-ordered structure of the metal hydroxide layers was at least partially destroyed [59]. These results are in agreement with the values of Flory-Huggins interaction parameters between the LDPE and organo-LDHs. Actually, the interaction between the LDPE and organo-LDHs can be estimated according to the method reported in the literature and based on the determination of solubility parameters using the molar attraction constants of the functional groups derived from the Hoy's table [60, 61]. In particular, the solubility parameters of LDPE and organo-LDHs can be calculated according to the following Equation (5):

$$\delta = \frac{\rho \Sigma F_i}{M} \tag{5}$$

where δ is the solubility parameter of the species, ΣF_i is the sum of the molar attraction constants of all the groups in the repeating unit of the species, M is the molecular weight of the repeating unit, and ρ is the density of the species. The solubility parameters for LDPE and LDH-C6, LDH-C12 and LDH-C20 are 18.0, 16.3, 16.9 and 17.1 $J^{1/2} \cdot cm^{-3/2}$. Hence, the Flory-Huggins interaction parameter (χ_{AB}) between two components (A and B) can be calculated as shown in Equation (6):

$$(\delta_A - \delta_B)^2 = \frac{\chi_{AB} RT}{V_r} \tag{6}$$

where R is the gas constant, T is the temperature and V_r is a reference volume (which can be considered to be 100 $cm^3 \cdot mol^{-1}$). In particular, the χ_{AB} value for LDPE and LDH-20 (0.03) is smaller than for LDPE and LDH-12 (0.05) and LDPE and LDH-6

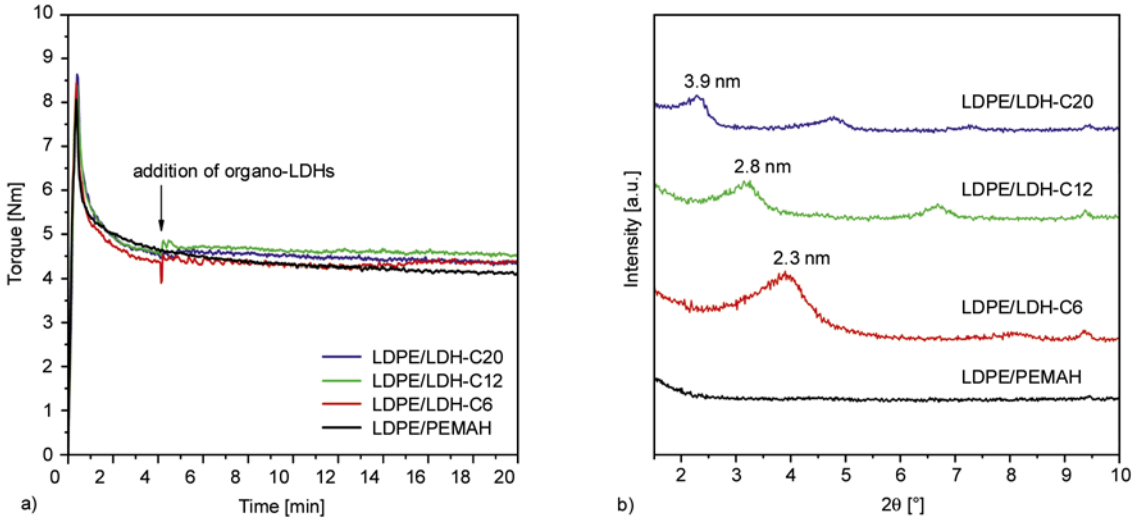

Figure 7. Torque vs. time plot during melt mixing (a) and XRD patterns (b) of the LDPE/organo-LDH composites

(0.12), thus indicating an interaction more thermodynamically favorable, even if in all the three cases the values are rather low.

To have a clearer overview of the dispersion of the LDH platelets, SEM images were acquired on the fractured surfaces of the samples (Figure 8a–c). In the case of the LDPE/LDH-C6 composite (Figure 8a), both low and high magnification SEM images evidenced the presence of aggregates of LDH-C6 platelets of 2 to 3 μm, whereas, in the case of composites containing LDH-C12 (Figure 8b) and LDH-C20 (Figure 8c), the aggregates have lower dimensions (see high magnification images; particles pointed to by arrows) and the LDH particles

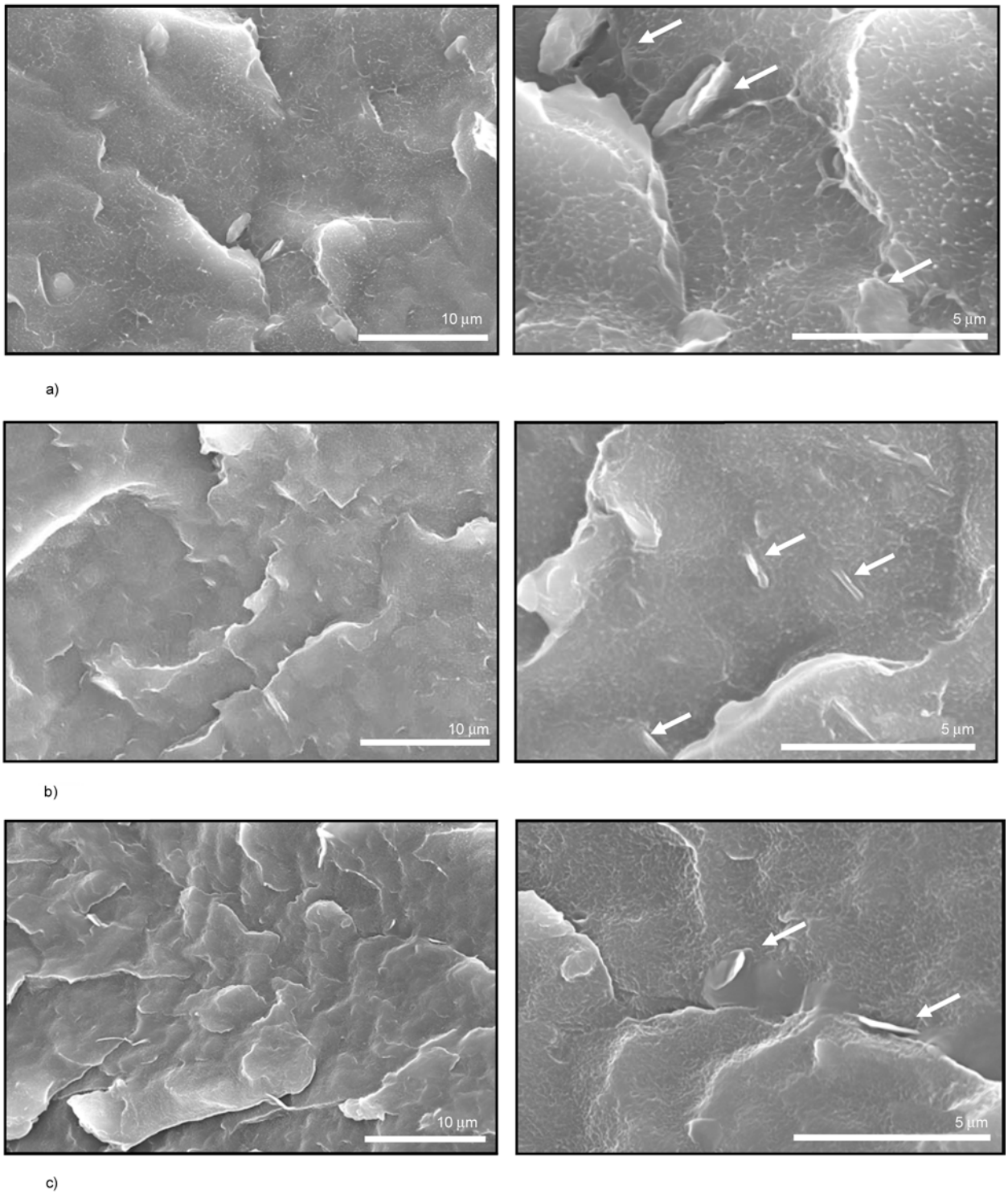

Figure 8. SEM micrographs of the composites: (a) LDPE/LDH-C6; (b) LDPE/LDH-C12; and (c) LDPE/LDH-C20, at low (3000×, left) and high (10000×, right) magnifications

seem to be better dispersed in the matrix. Moreover, no voids were observed between the intercalated particles and the matrix at the failure surface, which indicates that a strong interaction exists between them. Therefore, it seems that the dispersed platelets were well coated by the LDPE, probably thanks to the presence of PEMAH chains, which should promote favorable interactions with the LDH surface.

By combining the XRD and SEM results, it appears that the extent of the organo-LDH dispersion in the LDPE depends 'primarily' on the interlayer distance of the organo-LDHs and, therefore, on the chain length of the anionic modifiers and their assembly between the LDH layers. Moreover, the favorable interactions between the organo-LDHs and the polymer matrix promote intercalation, dispersion and adhesion. Actually, the increase of the *d*-spacing and, therefore the formation of intercalated structures, was preferentially observed when the number of carbon atoms of the surfactant alkyl chain is equal to or larger than 12. To deeply investigate the morphology of the LDPE/LDH-C12 sample, TEM images were acquired (Figure 9). As already indicated by SEM analysis, micrometric particles of different dimensions up to more than 10 μm, may be formed by assembling of intercalated tactoids, were observed into the matrix. Furthermore, neither submicrometer tactoids nor single lamellae were detected.

On the basis of these results, it can be reasonably supposed that during melt processing, polymer chains preferentially intercalate between the LDH sheets of the organo-LDHs having the highest *d*-spacing values (LDH-C12 and LDH-C20), likely also as a consequence of better interactions between the long chain surfactants and the PE; but intercalation was not sufficient to obtain high degrees of delamination and dispersion of platelets.

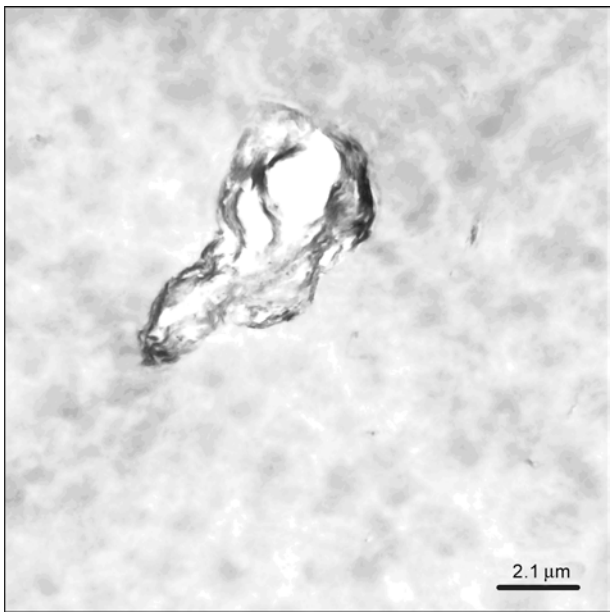

Figure 9. TEM image of the LDPE/LDH-C12 sample

Generally, the properties of nanocomposites prepared with organo-clays are improved or depressed when the amount of filler is increased. In order to investigate this aspect, LDH-C12 was selected for preparing an additional organo-LDH/LDPE composite with 5 wt% of organo-LDH with respect to the polymers (LDPE/LDH-C12_5%). The XRD pattern of this new sample evidenced a broad diffraction peak at $2\theta = 3.4°$ ($d_{003} = 2.7$ nm), slightly more shifted toward the (003) reflection of the pristine LDH-C12 with respect to the reflection detected in the case of the 2.5 wt% composite (Figure 10a).

This result could be a consequence of the presence of non-intercalated LDH-C12 platelets. Actually, low and high magnification SEM images (Figure 10b) evidenced the presence of numerous aggregates with a size of about 2 to 5 μm, most likely made of several interconnected LDH platelets. It seems that these big particles are kept together by strong face-face interactions between adjacent LDH platelets (indicated by the circle) or between individual layers.

The TGA and DTG curves of the LDPE, LDPE/PEMAH, and organo-LDH composites are shown in Figure 11. The temperatures corresponding to 10 and 50% of weight loss ($T_{10\%}$ and $T_{50\%}$), the temperature at the maximum rate of weight loss (T_{max}), and the residue obtained at 900°C are reported in Table 2. A two-step decomposition is apparent for the composites: the first step, in the temperature range of 200 to 405°C (□25% weight loss), involves the dehydration of metal hydroxide layers, thermal degradation of the organic modifiers, and volatilization of the thermo-oxidative products of LDPE [33]; the second step, in the temperature range of 405 to 600°C (□70−75% weight loss), is ascribed to the decomposition of polyethylene chains and the volatilization of the residual polymer [62]. It can be observed that the initial degradation (i.e. at 10% weight loss of composites) is faster, compared to the pure matrix, which is due to the earlier degrada-

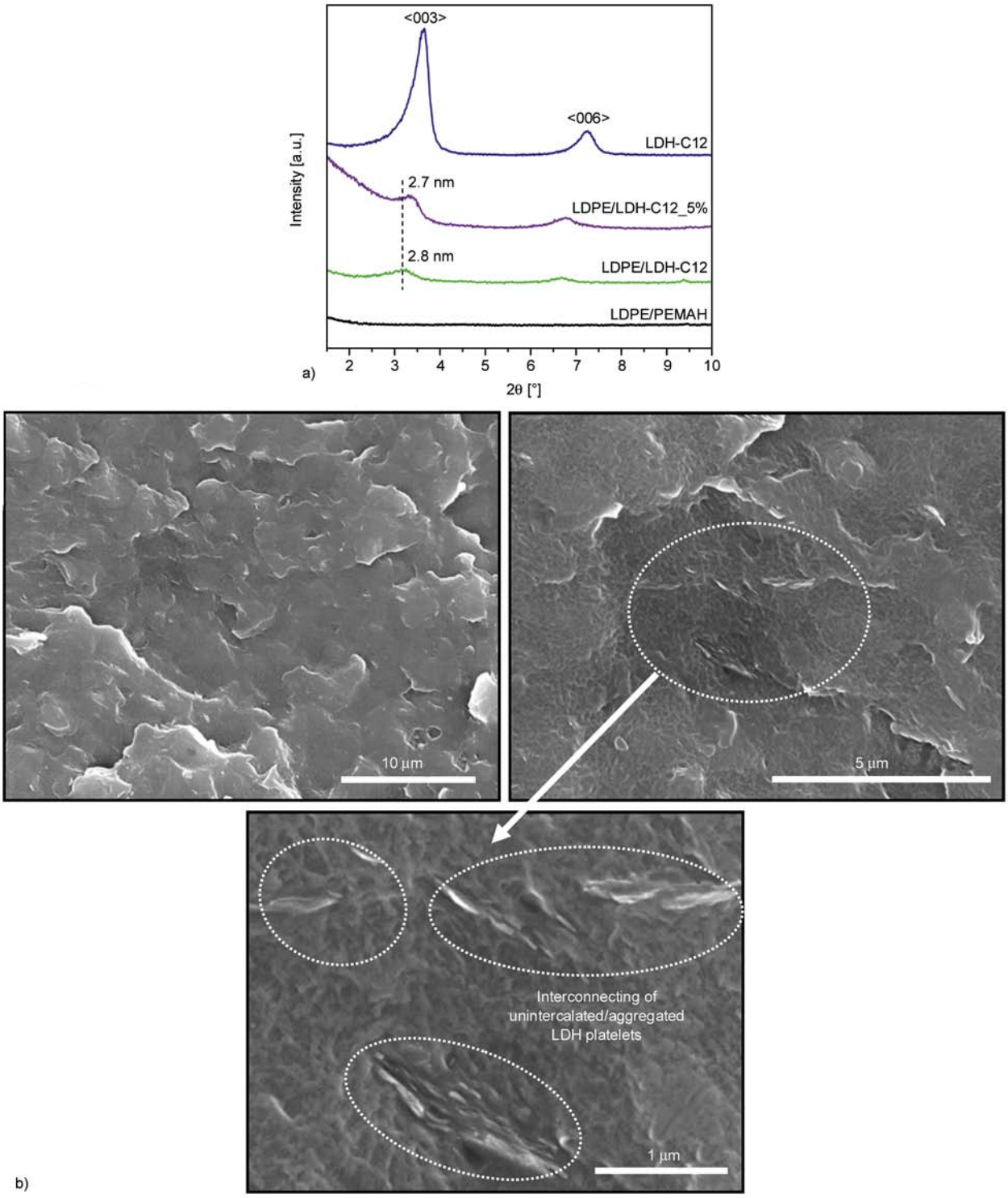

Figure 10. Comparison of the XRD patterns of LDPE/LDH-C12 and the LDPE/LDH-C12_5% composites (a) and low and high magnification SEM images of the LDPE/LDH-C12_5% composite (b)

tion of the organic modifiers [34, 37]. However, the layers produced by the fast degradation of the organo-LDHs are very advantageous for promoting the charring process, thus enhancing the thermal stability of the polymer materials. This remarkable enhancement of thermal properties is characterized by a shift of the TGA and DTG curves (Figure 11b) toward higher temperatures, after 25% weight loss, and the temperature at the maximum rate of weight loss (T_{max}) is increased by about 20 to 33°C with respect to the pure matrix, suggesting a generally slower degradation process. Among these compos-

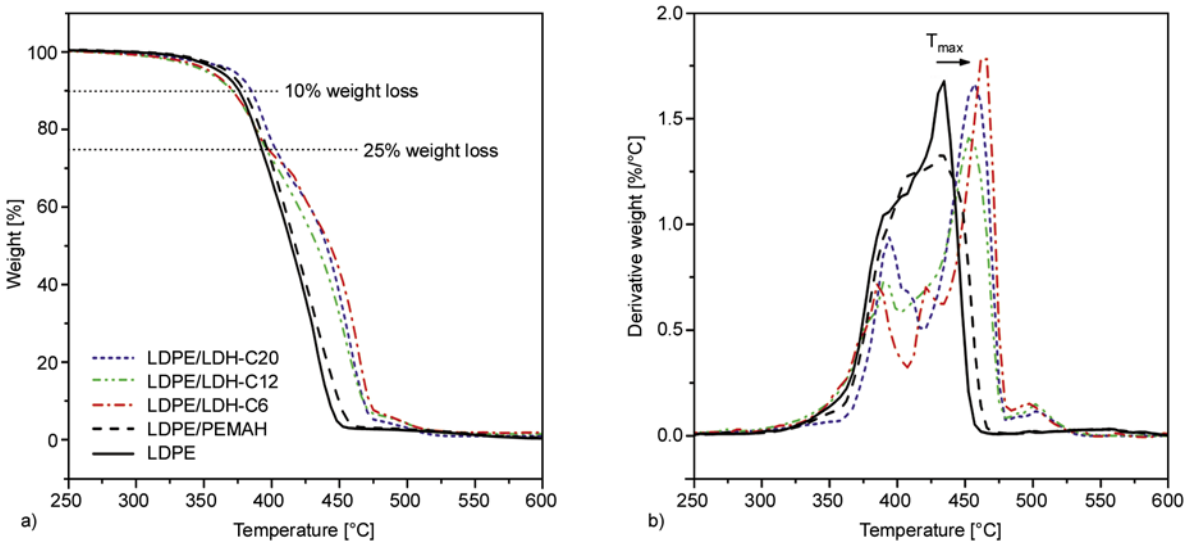

Figure 11. TGA (a) and DTG (b) thermograms of the LDPE/organo-LDH composites

ites, the LDPE/LDH-C6 sample has the highest degradation temperature, even though the XRD and SEM analyses evidenced a poor dispersion degree. However, the degradation temperature of the LDPE/LDH-C20 is nearly the same as that of the LDPE/LDH-C6, even if a lower amount of clay was added to the LDPE/LDH-C20 sample (1.5 wt% with respect to the LDPE/PEMAH blend). This infers that LDH platelets in the bulk polymer promote the charring process and enhance the flame retardant properties of the LDPE [36, 37, 63].

The residue left after combustion of LDPE and LDPE/PEMAH blend is nearly zero as the hydrocarbon chains are converted into gaseous products. If we assume that by heating up the composites to 900°C under air both the polymers and the organic part of organo-LDHs are completely burnt, the amount of TGA residue could be deduced from the organo-LDH formulae. Actually, by considering the formation of metal oxides, the residue is proportional to the amount of organo-LDH added to the polymer blends.

The melting (T_m) and crystallization (T_c) peak temperatures, as well as the melting enthalpy (ΔH_m) and degree of crystallinity (χ_c), were determined by DSC measurements (Table 2).

Most of the samples show an increase of T_c, especially in the case of LDPE/LDH-C20, and a slight decrease of T_m with respect to the LDPE/PEMAH blend. The increase of T_c is probably due to the heterogeneous nucleation activity of the dispersed LDH platelets; actually, just a small amount of the LDH platelets could accelerate the crystallization process of LDPE. However, the degree of crystallinity seems unchanged and independent of the type of composite. By comparing the two LDPE composites prepared with different concentrations of LDH-C12, it can be observed that there was no significant influence of the amount of organo-LDH on the crystallization and melting behavior of LDPE. Instead, a slight decrease of degree of crystallinity (χ_c, Table 2) is observed; this decrease is probably due to the suppression effect of the aggregated-LDH, which hinders the growth of the LDPE crystallites.

The storage modulus (E'), loss modulus (E'') and loss tangent (tanδ) behavior vs. temperature of composites prepared with the different types of organo-LDHs are shown in Figure 12a–c.

Generally, LDPE exhibits three relaxations (known as α, β and γ) which are associated with chain motions in the crystalline phase (α at about +50°C), chain motions of branched structures in the amorphous matrix (the β-relaxation, at about –20°C, is absent in entirely linear polyethylene), and the motion of the amorphous polyethylene which is caused by small local short-range segmental motions involving three to five CH_2 chain segments (γ at about –125°C) [64, 65]. It can be observed from Figure 12a that the E' of all of the samples decreases slowly until –50°C; then a sharp drop appears, which is related to the β-relaxation process. The E' of the composites is higher than that of the LDPE/PEMAH matrix in the low temperature region

(Table 3), except in the case of the LDPE/LDH-C20 sample.

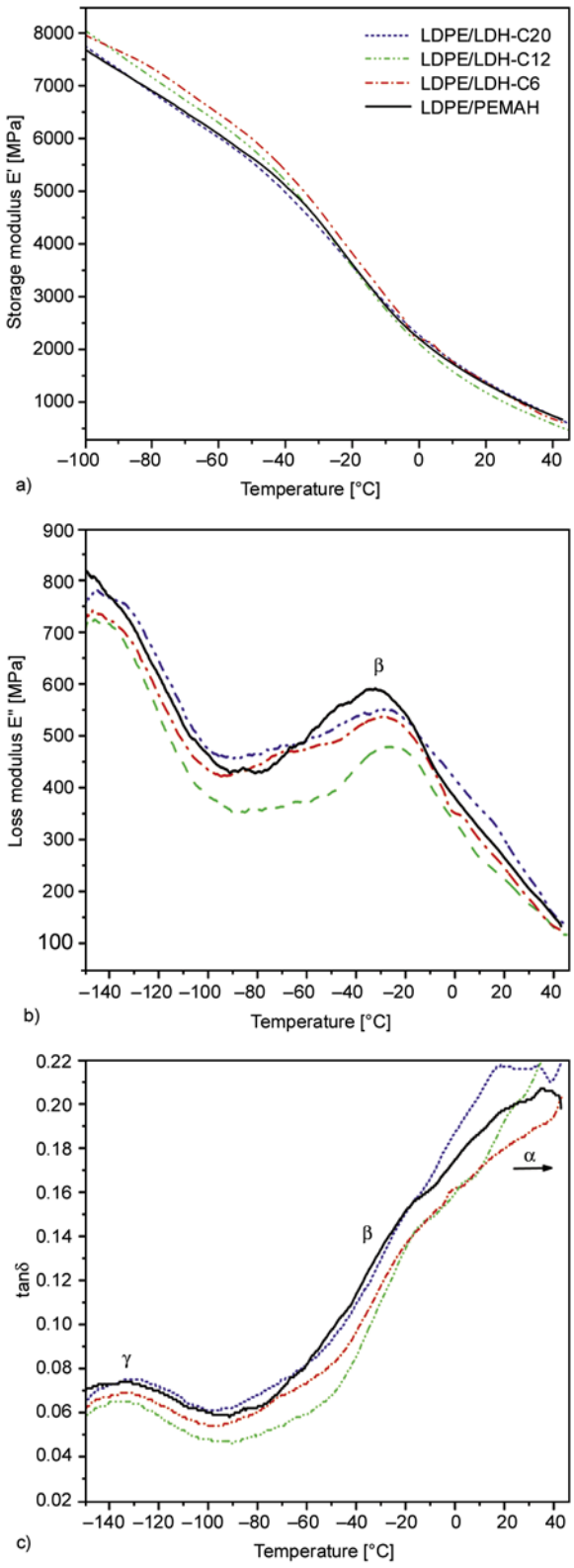

Figure 12. Dynamic (a) storage modulus, (b) loss modulus, and (c) loss tangent of the pure matrix and the LDPE/organo-LDH composites

In a previous work, it was found that LDPE/organo-LDH nanocomposites, prepared in a twin screw extruder, had a lower storage modulus with respect to the polymer matrix [41], not evidencing reinforcement, but rather a softening of the matrix. It was assumed that this effect could be a consequence of the low stiffness of the organo-LDH particles [66–68], even if it was not excluded that the free surfactant and surfactant molecules loosely bound to the outer surface of the LDH particles could increase the mobility of the polymer chains at the polymer-filler interfacial region, thus acting as plasticizers [68]. On the basis of the results collected here, it can be assumed that higher values of E' are probably obtained when the organo-LDH dispersion is poor. Actually, the highest E' was achieved for the LDPE/LDH-C6 sample, which has the worst dispersion morphology, as evidenced by the XRD and SEM characterizations. Nonetheless, it cannot be excluded that, independently of morphology, the surfactant chain could act as a plasticizer, increasing the mobility of the polymer chains at the polymer-filler interfacial region; the longer the alkyl chain, the higher the extent of the surfactant-polymer interaction as demonstrated by the calculation of interaction parameters, and greater the efficiency of the surfactant as plasticizer. This means that the different lengths of the surfactant alkyl chain play a fundamental role, not only related to the dispersion/morphology aspects, but also to the interactions at the interface, thus very much affecting the final properties.

The β-relaxation is assumed here to be the glass transition temperature (T_g) of the composite. Indeed, it is reported that both the γ- and β-relaxations are quoted to have the properties of the glass–rubber transition. In particular, when the alkylidene content is low, the γ-peak is more prominent, whereas β-relaxation is the dominant mechanism at high alkylidene content. It has been also shown that the higher the amorphous fraction, the more intense is the β-relaxation, which may be classified as T_g [64, 65]. It appears from Figure 12b–c that the peak position related to the β-relaxation of the composites shifts to higher temperatures compared to that of the LDPE.

Generally the state of dispersion of clay platelets in polymer nanocomposite systems is determined by dynamic oscillatory shear measurements. Actually,

Table 3. Dynamic storage modulus and peak temperature of β and γ relaxations for the pure matrix and the LDPE/organo-LDH composites

Composites	Storage modulus, E', [MPa]			Relaxations peak temperature [°C]	
	–100°C	–80°C	–60°C	β	γ
LDPE/PEMAH	7704.8	6911.1	6108.8	–33.6	–133.5
LDPE/LDH-C6 (2.5 wt%)	7997.7	7353.6	6479.8	–27.6	–132.2
LDPE/LDH-C12 (2.5 wt%)	8075.8	7163.6	6304.1	–25.6	–133.0
LDPE/LDH-C20 (1.5 wt%)	7782.9	6911.1	6030.8	–27.1	–129.2
LDPE/LDH-C12_5% (5.0 wt%)	8238.9	7477.6	6712.0	–27.8	–132.0

the storage (G') and loss moduli (G'') of the nanocomposites increases monotonically with the clay loading at all frequencies, but beyond a threshold volume fraction, the individual layers and tactoids are not able to rotate freely, and thus incomplete relaxation occurred when subjected to the shear. This incomplete relaxation due to the physical jamming or to the formation of a percolated three dimensional network leads to the presence of the pseudo-solid-like behavior observed in both intercalated and exfoliated nanocomposites [69, 70]. It is suggested that the strong interaction between the polymer and the clay platelets restricts the mobility and alters the relaxation processes of the polymer, leading to the low-frequency plateau in the shear moduli and non-Newtonian viscosity behavior with clay loading at the low-shear rate [71]. These measurements also showed that tanδ (G''/G') is dependent on polymer-clay interaction; in particular, tan$\delta > 3$ for non-associated, $1 <$ tan$\delta < 3$ for weakly associated, and tan$\delta < 1$ for strongly associated dispersed particles [72]. Hyun *et al.* [73] also evidenced that the clay content affects the tanδ value: at low clay content tanδ is greater than 1, while at high clay content tanδ becomes less than 1. In our case, the height of the tan δ peak of the composites (Figure 12c) decreases with respect to the matrix, moving from the composite prepared by adding LDH-C20 to LDH-C12 and to LDH-C6. The tanδ values for the β-relaxation (–40°C) are for all the samples much smaller than 1: LDPE/PEMAH = 0.114, LDH-C6 = 0.097, LDH-C12 = 0.088 and to LDH-C20 = 0.110. This suggests the presence of strongly associated dispersed platelets, which supports the formation of intercalated composites, as shown by XRD results and confirmed by the large rigid aggregates evidenced by SEM images. It can be also observed that tanδ curves after room temperature seem to move to higher temperature, which is correlated to the α-relaxation region. Most likely the polymer−clay interactions not only restricted the molecular motion in the amorphous phase, but also confined the segmental relaxation in the crystalline phase [64]. A similar behavior was observed on other systems such as EVA/EPDM/DS-LDH nanocomposites [67] and PBT nanocomposites [68].

By increasing the LDH concentration of the composites (LDPE/LDH-C12_5% vs. LDPE/LDH-C12) a higher E' value was observed throughout the entire temperature range (Table 3), thus suggesting that the addition of the LDH enhanced the stiffness of the composite. The temperature dependence of the storage modulus enhancement factor, defined as $E'_{real} = E'_{composite}/E'_{pure}$ matrix, in the case of the LDPE/LDH-C12 (2.5 wt%) and LDPE/LDH-C12_5% (5 wt%) composites, is shown in Figure 13.

By increasing the amount of LDH-C12, the relative storage modulus is increased. This may contribute to the fact that some volume of the composite is occupied by LDH particles, for which the storage modulus is much greater than for the pure polymer.

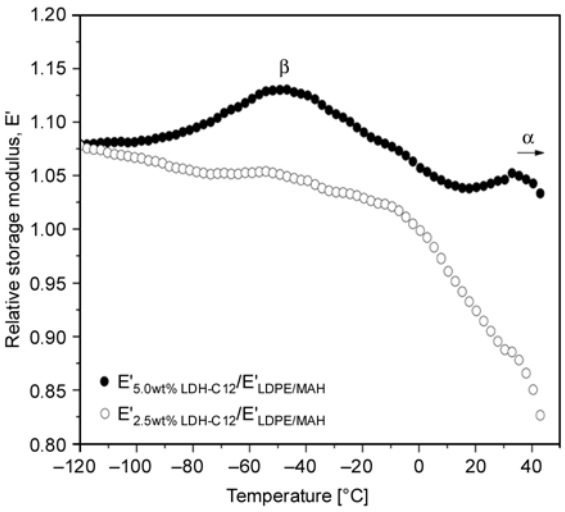

Figure 13. Temperature dependence of relative storage modulus ($E'_{composite}/E'_{pure\ matrix}$) for the 2.5 and 5 wt% LDH-C12 composites.

In that case, two distinct peaks appear at –46 and 33°C, which are related to the setting up of the chain motion in the amorphous (β-relaxation) and crystalline (α-relaxation) phases, respectively. In the case of the LDPE/LDH-C12 (2.5 wt%) sample, the relative modulus curve is nearly constant from the beginning until –10°C, and afterward it suddenly drops. The observed glass transition temperature (T_g) of the LDPE/LDH-C12_5% (5 wt%) sample slightly decreases compared to that of LDPE/LDH-C12, but it is much higher than that of the pure matrix (see Table 3). Moreover, as already been suggested about the tanδ value for higher clay loading, the composite with 5 wt% LDH-C12 shows the strongly associated dispersed clay platelets with tanδ less than 1 (0.087).

4. Conclusions

LDPE/organo-LDH composites were prepared via melt-compounding using PEMAH as the compatibilizer. Pristine LDH-CO_3 was modified with various alkyl chain length sulfates (n_c = 6, 12 and 20) by a two step anion exchange methodology. The XRD analysis demonstrated that intercalated LDPE/organo-LDH composites were obtained by melt mixing, depending on the chain length of the anionic modifiers. In particular, intercalated structures were achieved when the number of carbon atoms of the surfactant alkyl chain was equal to or larger than 12. Moreover, the TGA analysis showed that the composites exhibited a remarkable enhancement of thermal properties, in which the decomposition temperature is 20 to 33°C higher than that of the pure matrix. The DSC results showed an increase of the crystallization temperature, due mainly to nucleation effects, whereas, neither significant changes of the melting temperature nor of the degree of crystallinity were observed. On the other hand, the mechanical properties, and in particular the storage modulus data, were affected by the morphology and by the physical properties of the surfactants at the interface. Generally, a reinforcing effect was observed by using LDH modified by surfactants having short alkyl chains (C6), providing larger aggregates owing to a sort of physical crosslinking effect induced by the strong interactions between the functionalized polymer and the layered clay. The significant increase of the β-relaxation peak temperature related to the glass transition temperature (T_g) of the composites may be explained by the stronger interactions between the polymer and the layered filler, which restricted the mobility of the polymer chains. By increasing the chain length of the LDH modifier, a softening of the composite was observed due to a plasticizing effect of the surfactant, which also promoted effective interactions between the matrix and the nanofiller, thus providing a better morphology. This means that the alkyl chain length of the surfactant could play a fundamental role, not only related to the dispersion/morphology aspects, but also to the interactions at the interface, very much affecting the final properties.

Acknowledgements

The research was funded by the Department of Chemistry and Industrial Chemistry, University of Pisa, the National Project PRIN prot. 200898KCKY, and the Royal Golden Jubilee Ph.D. Program (RGJ). The authors express their appreciation to Prof. Francesco Ciardelli for the helpful discussion and support. Dr. Lucia Conzatti (CNR-ISMAC UOS Genova, Genova, Italy) is gratefully acknowledged for her cooperation about TEM analysis.

References

[1] Brown G., Gastuche M. C.: Mixed magnesium-aluminum hydroxides. II. Structure and structural chemistry of synthetic hydroxycarbonates and related minerals and compounds-II. Clay Minerals, **7**, 193–201 (1967).

[2] Miyata S., Kumara T.: Synthesis of new hydrotalcite-like compounds and their physico-chemical properties. Chemistry Letters, **2**, 843–848 (1973). DOI: 10.1246/cl.1973.843

[3] Cavani F., Trifirò F., Vaccari A.: Hydrotalcite-type anionic clays: Preparation, properties and applications. Catalysis Today, **11**, 173–301 (1991). DOI: 10.1016/0920-5861(91)80068-K

[4] Reichle W. T.: Synthesis of anionic clay minerals (mixed metal hydroxides, hydrotalcite). Solid State Ionics, **22**, 135–141 (1986). DOI: 10.1016/0167-2738(86)90067-6

[5] Auerbach S. M., Carrado K., Dutta P. K.: Handbook of layered materials. Marcel Dekker, New York (2004).

[6] Constantino V. R. L., Pinnavaia T. J.: Basic properties of $Mg^{2+}_{1-x}Al^{3+}_{x}$ layered double hydroxides intercalated by carbonate, hydroxide, chloride, and sulfate anions. Inorganic Chemistry, **34**, 883–892 (1995). DOI: 10.1021/ic00108a020

[7] del Arco M., Malet P., Trujillano R., Rives V.: Synthesis and characterization of hydrotalcites containing Ni(II) and Fe(III) and their calcination products. Chemistry of Materials, **11**, 624–633 (1999). DOI: 10.1021/cm9804923

[8] Xu Z. P., Zeng H. C.: Thermal evolution of cobalt hydroxides: A comparative study of their various structural phases. Journal of Materials Chemistry, **8**, 2499–2506 (1998).
DOI: 10.1039/A804767G

[9] Hermosín M. C., Pavlovic J., Ulibarri M. A., Cornejo J.: Hydrotalcite as sorbent for trinitrophenol: Sorption capacity and mechanism. Water Research, **30**, 171–177 (1996).
DOI: 10.1016/0043-1354(95)00088-3

[10] Qian M., Zeng H. C.: Synthesis and characterization of Mg–Co catalytic oxide materials for low-temperature N_2O decomposition. Journal of Materials Chemistry, **7**, 493–499 (1997).
DOI: 10.1039/A607627K

[11] Ambrogi V., Fardella G., Grandolini G., Perioli L.: Intercalation compounds of hydrotalcite-like anionic clays with antiinflammatory agents – I. Intercalation and in vitro release of ibuprofen. International Journal of Pharmaceutics, **220**, 23–32 (2001).
DOI: 10.1016/S0378-5173(01)00629-9

[12] Guo X., Xu S., Zhao L., Lu W., Zhang F., Evans D. G., Duan X.: One-step hydrothermal crystallization of a layered double hydroxide/alumina bilayer film on aluminum and its corrosion resistance properties. Langmuir, **25**, 9894–9897 (2009).
DOI: 10.1021/la901012w

[13] Luan L., Li W., Liu S., Sun D.: Phase behavior of mixtures of positively charged colloidal platelets and nonadsorbing polymer. Langmuir, **25**, 6349–6356 (2009).
DOI: 10.1021/la804023b

[14] Crepaldi E. L., Pavan P. C., Valim J. B.: Anion exchange in layered double hydroxides by surfactant salt formation. Journal of Materials Chemistry, **10**, 1337–1343 (2000).
DOI: 10.1039/A909436I

[15] Costa F. R., Saphiannikova M., Wagenknecht U., Heinrich G.: Layered double hydroxide based polymer nanocomposites. Advances in Polymer Science, **210**, 101–168 (2008).
DOI: 10.1007/12_2007_123

[16] Ciardelli F., Coiai S., Passaglia E., Pucci A., Ruggeri G.: Nanocomposites based on polyolefins and functional thermoplastic materials. Polymer International, **57**, 805–836 (2008).
DOI: 10.1002/pi.2415

[17] Wang D-Y., Costa F. R., Vyalikh A., Leuteritz A., Scheler U., Jehnichen D., Wagenknecht U., Haussler L., Heinrich G.: One-step synthesis of organic LDH and its comparison with regeneration and anion exchange method. Chemistry of Materials, **21**, 4490–4497 (2009).
DOI: 10.1021/cm901238a

[18] Newman S. P., Jones W.: Synthesis, characterization and applications of layered double hydroxides containing organic guests. New Journal of Chemistry, **22**, 105–115 (1998).
DOI: 10.1039/A708319J

[19] Miyata S.: Anion-exchange properties of hydrotalcite-like compounds. Clays and Clay Minerals, **31**, 305–311 (1983).
DOI: 10.1346/CCMN.1983.0310409

[20] Hsueh H-B., Chen C-Y.: Preparation and properties of LDHs/epoxy nanocomposites. Polymer, **44**, 5275–5283 (2003).
DOI: 10.1016/S0032-3861(03)00579-2

[21] Hsueh H-B., Chen C-Y.: Preparation and properties of LDHs/polyimide nanocomposites. Polymer, **44**, 1151–1161 (2003).
DOI: 10.1016/S0032-3861(02)00887-X

[22] Lee W. D., Im S. S., Lim H-M., Kim K-J.: Preparation and properties of layered double hydroxide/poly(ethylene terephthalate) nanocomposites by direct melt compounding. Polymer, **47**, 1364–1371 (2006).
DOI: 10.1016/j.polymer.2005.12.056

[23] Messersmith P. B., Stupp S. I.: High-temperature chemical and microstructural transformations of a nanocomposite organoceramic. Chemistry of Materials, **7**, 454–460 (1995).
DOI: 10.1021/cm00051a004

[24] Wang D-Y., Leuteritz A., Wang Y-Z., Wagenknecht U., Heinrich G.: Preparation and burning behaviors of flame retarding biodegradable poly(lactic acid) nanocomposite based on zinc aluminum layered double hydroxide. Polymer Degradation and Stability, **95**, 2474–2480 (2010).
DOI: 10.1016/j.polymdegradstab.2010.08.007

[25] Costantino U., Bugatti V., Gorrasi G., Montanari F., Nocchetti M., Tammaro L., Vittoria V.: New polymeric composites based on poly(ε-caprolactone) and layered double hydroxides containing antimicrobial species. Applied Materials and Interfaces, **1**, 668–677 (2009).
DOI: 10.1021/am8001988

[26] Ding P., Qu B.: Synthesis of exfoliated PP/LDH nanocomposites via melt-intercalation: Structure, thermal properties, and photo-oxidative behavior in comparison with PP/MMT nanocomposites. Polymer Engineering and Science, **46**, 1153–1159 (2006).
DOI: 10.1002/pen.20568

[27] Kuppinger J., Göschel U., Reeksting B., Vorster O.: Maleic anhydride grafted polypropylene-layered hydrotalcite master batch and resultant nanocomposites prepared by melt processing: Structure characterization and mechanical properties. Journal of Polymer Engineering, **27**, 339–356 (2007).

[28] Coiai S., Passaglia E., Hermann A., Augier S., Pratelli D., Streller R. C.: The influence of the compatibilizer on the morphology and thermal properties of polypropylene-layered double hydroxide composites. Polymer Composites, **31**, 744–754 (2010).
DOI: 10.1002/pc.20857

[29] Wang D-Y., Das A., Costa F. R., Leuteritz A., Wang Y-Z., Wagenknecht U., Heinrich G.: Synthesis of organo cobalt–aluminum layered double hydroxide via a novel single-step self-assembling method and its use as flame retardant nanofiller in PP. Langmuir, **26**, 14162–14169 (2010).
DOI: 10.1021/la102449m

[30] Wang D-Y., Das A., Leuteritz A., Boldt R., Häußler L., Wagenknecht U., Heinrich G.: Thermal degradation behaviors of a novel nanocomposite based on polypropylene and Co-Al layered double hydroxide. Polymer Degradation and Stability, **96**, 285–290 (2011).
DOI: 10.1016/j.polymdegradstab.2010.03.003

[31] Chen W., Qu B.: Structural characteristics and thermal properties of PE-g-MA/MgAl-LDH exfoliation nanocomposites synthesized by solution intercalation. Chemistry of Materials, **15**, 3208–3213 (2003).
DOI: 10.1021/cm030044h

[32] Chen W., Qu B.: LLDPE/ZnAl LDH-exfoliated nanocomposites: Effects of nanolayers on thermal and mechanical properties. Journal of Materials Chemistry, **14**, 1705–1710 (2004).
DOI: 10.1039/B401790K

[33] Chen W., Feng L., Qu B.: Preparation of nanocomposites by exfoliation of ZnAl layered double hydroxides in nonpolar LLDPE solution. Chemistry of Materials, **16**, 368–370 (2004).
DOI: 10.1021/cm0303484

[34] Qiu L., Chen W., Qu B.: Morphology and thermal stabilization mechanism of LLDPE/MMT and LLDPE/LDH nanocomposites. Polymer, **47**, 922–930 (2006).
DOI: 10.1016/j.polymer.2005.12.017

[35] Costa F. R., Abdel-Goad M., Wagenknecht U., Heinrich G.: Nanocomposites based on polyethylene and Mg–Al layered double hydroxide. I. Synthesis and characterization. Polymer, **46**, 4447–4453 (2005).
DOI: 10.1016/j.polymer.2005.02.027

[36] Costa F. R., Wagenknecht U., Heinrich G.: LDPE/Mg–Al layered double hydroxide nanocomposite: Thermal and flammability properties. Polymer Degradation and Stability, **92**, 1813–1823 (2007).
DOI: 10.1016/j.polymdegradstab.2007.07.009

[37] Du L., Qu B.: Structural characterization and thermal oxidation properties of LLDPE/MgAl-LDH nanocomposites. Journal of Materials Chemistry, **16**, 1549–1554 (2006).
DOI: 10.1039/B514319E

[38] Costantino U., Gallipoli A., Nocchetti M., Camino G., Bellucci F., Frache A.: New nanocomposites constituted of polyethylene and organically modified ZnAl-hydrotalcites. Polymer Degradation and Stability, **90**, 586–590 (2005).
DOI: 10.1016/j.polymdegradstab.2005.05.019

[39] Costa F. R., Wagenknecht U., Jehnichen D., Goad M. A., Heinrich G.: Nanocomposites based on polyethylene and Mg–Al layered double hydroxide. Part II. Rheological characterization. Polymer, **47**, 1649–1660 (2006).
DOI: 10.1016/j.polymer.2005.12.011

[40] Manzi-Nshuti C., Hossenlopp J. M., Wilkie C. A.: Comparative study on the flammability of polyethylene modified with commercial fire retardants and a zinc aluminum oleate layered double hydroxide. Polymer Degradation and Stability, **94**, 782–788 (2009).
DOI: 10.1016/j.polymdegradstab.2009.02.004

[41] Coiai S., Scatto M., Conzatti L., Azzurri F., Andreotti L., Salmini E., Stagnaro P., Zanolin A., Cicogna F., Passaglia E.: Optimization of organo-layered double hydroxide dispersion in LDPE-based nanocomposites. Polymer for Advanced Technologies, in press (2011).
DOI: 10.1002/pat.1759

[42] Costa F. R., Satapathy B. K., Wagenknecht U., Weidisch R., Heinrich G.: Morphology and fracture behaviour of polyethylene/Mg–Al layered double hydroxide (LDH) nanocomposites. European Polymer Journal, **42**, 2140–2152 (2006).
DOI: 10.1016/j.eurpolymj.2006.04.005

[43] Tammaro L., Tortora M., Vittoria V., Costatino U., Marmottini F.: Methods of preparation of novel composites of poly(ε-caprolactone) and a modified Mg/Al hydrotalcite. Journal of Polymer Science Part A: Polymer Chemistry, **43**, 2281–2290 (2005).
DOI: 10.1002/pola.20701

[44] Zammarano M., Bellayer S., Gilman J. W., Franceschi M., Beyer F. L., Harris R. H., Meriani S.: Delamination of organo-modified layered double hydroxides in polyamide 6 by melt processing. Polymer, **47**, 652–662 (2006).
DOI: 10.1016/j.polymer.2005.11.080

[45] Zammarano M., Franceschi M., Bellayer S., Gilman J. W., Meriani S.: Preparation and flame resistance properties of revolutionary self-extinguishing epoxy nanocomposites based on layered double hydroxides. Polymer, **46**, 9314–9328 (2005).
DOI: 10.1016/j.polymer.2005.07.050

[46] Velu S., Ramkumar V., Narayanan V., Swamy C. S.: Effect of interlayer anions on the physicochemical properties of zinc–aluminium hydrotalcite-like compounds. Journal of Materials Science, **32**, 957–964 (1997).
DOI: 10.1023/A:1018561918863

[47] Kopka H., Beneke K., Lagaly G.: Anionic surfactants between double metal hydroxide layers. Journal of Colloid and Interface Science, **123**, 427–436 (1988).
DOI: 10.1016/0021-9797(88)90263-9

[48] Meyn M., Beneke K., Lagaly G.: Anion-exchange reactions of layered double hydroxides. Inorganic Chemistry, **29**, 5201–5207 (1990).
DOI: 10.1021/ic00351a013

[49] Meyn M., Beneke K., Lagaly G.: Anion-exchange reactions of hydroxy double salts. Inorganic Chemistry, **32**, 1209–1215 (1993).
DOI: 10.1021/ic00059a030

[50] You Y., Zhao H., Vance G. F.: Surfactant-enhanced adsorption of organic compounds by layered double hydroxides. Colloids and Surfaces A: Physicochemical and Engineering Aspects, **205**, 161–172 (2002).
DOI: 10.1016/S0927-7757(01)01137-2

[51] Carlino S.: The intercalation of carboxylic acids into layered double hydroxides: A critical evaluation and review of the different methods. Solid State Ionics, **98**, 73–84 (1997).
DOI: 10.1016/S0167-2738(96)00619-4

[52] Costa F. R., Leuteritz A., Wagenknecht U.: Intercalation of Mg–Al layered double hydroxide by anionic surfactants: Preparation and characterization. Applied Clay Science, **38**, 153–164 (2008).
DOI: 10.1016/j.clay.2007.03.006

[53] Costa F. R., Leuteritz A., Wagenknecht U., Auf der Landwehr M., Jehnichen D., Haussler L., Heinrich G.: Alkyl sulfonate modified LDH: Effect of alkyl chain length on intercalation behavior, particle morphology and thermal stability. Applied Clay Science, **44**, 7–14 (2009).
DOI: 10.1016/j.clay.2008.12.020

[54] Lagaly G., Beneke K.: Intercalation and exchange reactions of clay minerals and non-clay layer compounds. Colloid and Polymer Science, **269**, 1198–1211 (1991).
DOI: 10.1007/BF00652529

[55] Pavan P. C., Crepaldi E. L., Gomes G. D., Valim J. B.: Adsorption of sodium dodecylsulfate on a hydrotalcite-like compound. Effect of temperature, pH and ionic strength. Colloids and Surfaces A: Physicochemical and Engineering Aspects, **154**, 399–410 (1999).
DOI: 10.1016/S0927-7757(98)00847-4

[56] Aramendia M. A., Borau V., Jiménez C., Luque J. M., Marinas J. M., Ruiz J. R., Urbano F. J.: Epoxidation of limonene over hydrotalcite-like compounds with hydrogen peroxide in the presence of nitriles. Applied Catalysis A: General, **216**, 257–265 (2001).
DOI: 10.1016/S0926-860X(01)00570-1

[57] Kanezaki E.: Effect of atomic ratio Mg/Al in layers of Mg and Al layered double hydroxide on thermal stability of hydrotalcite-like layered structure BY means of in situ high temperature powder X-Ray diffraction. Materials Research Bulletin, **33**, 773–778 (1998).
DOI: 10.1016/S0025-5408(98)00021-X

[58] Durmus A., Kasgoz A., Macosko C. W.: Linear low density polyethylene (LLDPE)/clay nanocomposites. Part I: Structural characterization and quantifying clay dispersion by melt rheology. Polymer **48**, 4492–4502 (2007).
DOI: 10.1016/j.polymer.2007.05.074

[59] Vaia R. A., Liu W.: X-ray powder diffraction of polymer/layered silicate nanocomposites: Model and practice. Journal of Polymer Science Part B: Polymer Physics, **40**, 1590–1600 (2002).
DOI: 10.1002/polb.10214

[60] van Krevelen D. W., te Nijenhuis K.: Properties of polymers. Elsevier, Amsterdam (2009).

[61] Lim S-K., Hong E-P., Song Y-H., Park B. J., Jin H., Chin I-J.: Preparation and interaction characteristics of exfoliated ABS/organoclay nanocomposite. Polymer Engineering and Science, **50**, 504–512 (2010).
DOI: 10.1002/pen.21551

[62] Kashiwagi T., Gilman J. W., Nyden M. R., Lomakin S. M.: New intumescent polymeric materials polymer combustion and new flame retardants. in 'Fire retardancy of polymers. The use of intumescence' (eds: Le Bras M., Bourbigot S., Camino G.). The Royal Society of Chemistry, Cambridge, 175–202 (1998).

[63] Tang Y., Hu Y., Song L., Zong R., Gui Z., Chen Z., Fan W.: Preparation and thermal stability of polypropylene/montmorillonite nanocomposites. Polymer Degradation and Stability, **82**, 127–131 (2003).
DOI: 10.1016/S0141-3910(03)00173-3

[64] Hoffman J. D., Williams G., Passaglia E.: Analysis of the α, β, and γ relaxations in polychlorotrifluoroethylene and polyethylene: Dielectric and mechanical properties. Journal of Polymer Science Part C: Polymer Symposia, **14**, 173–235 (1966).
DOI: 10.1002/polc.5070140116

[65] Khanna Y. P., Turi E. A., Taylor T. J., Vickroy V. V., Abbott R. F.: Dynamic mechanical relaxations in polyethylene. Macromolecules, **18**, 1302–1309 (1985).
DOI: 10.1021/ma00148a045

[66] Xie Y., Yu D., Kong J., Fan X., Qiao W.: Study on morphology, crystallization behaviors of highly filled maleated polyethylene-layered silicate nanocomposites. Journal of Applied Polymer Science, **100**, 4004–4011 (2006).
DOI: 10.1002/app.23206

[67] Kuila T., Srivastava S. K., Bhowmick A. K.: Ethylene vinyl acetate/ethylene propylene diene terpolymer-blend-layered double hydroxide nanocomposites. Polymer Engineering and Science, **49**, 585–591 (2009).
DOI: 10.1002/pen.21286

[68] Berti C., Fiorini M., Sisti L.: Synthesis of poly(butylene terephtahlate) nanocomposites using anionic clays. European Polymer Journal, **45**, 70–78 (2009).
DOI: 10.1016/j.eurpolymj.2008.09.039

[69] Krishnamoorti R., Vaia R. A., Giannelis E. P.: Structure and dynamics of polymer-layered silicate nanocomposites. Chemistry of Materials, **8**, 1728–1734 (1996). DOI: 10.1021/cm960127g

[70] Ren J., Silva A. S., Krishnamoorti R.: Linear viscoelasticity of disordered polystyrene-polyisoprene block copolymer based layered-silicate nanocomposites. Macromolecules, **33**, 3739–3746 (2000). DOI: 10.1021/ma992091u

[71] Krishnamoorti R., Giannelis E. P.: Rheology of end-tethered polymer layered silicate nanocomposites. Macromolecules, **30**, 4097–4102 (1997). DOI: 10.1021/ma960550a

[72] Rohn C. L.: Analytical polymer rheology: Structure processing property relationships. Hanser, Munich (1995).

[73] Hyun Y. H., Lim S. T., Choi H. J., Jhon M. S.: Rheology of poly(ethylene oxide)/organoclay nanocomposites. Macromolecules, **34**, 8084–8093 (2001). DOI: 10.1021/ma002191w